Published in final edited form as:

Radiat Res. 2018 September ; 190(3): 236–247. doi:10.1667/RR15081.1.

Modeling Cell and Tumor-Metastasis Dosimetry with the Particle and Heavy Ion Transport Code System (PHITS) Software for Targeted Alpha-Particle Radionuclide Therapy

Dongyoul Lee[a], **Mengshi Li**[a], **Bryan Bednarz**[b], and **Michael K. Schultz**[a,c,d,e,f,g]

[a]Interdisciplinary Graduate Program in Human Toxicology, The University of Iowa, Iowa City, Iowa;

[b]Department of Medical Physics, University of Wisconsin, Madison, Wisconsin;

[c]Stead Family Department of Pediatrics, Carver College of Medicine, The University of Iowa, Iowa City, Iowa;

[d]Department of Radiology, Carver College of Medicine, The University of Iowa, Iowa City, Iowa;

[e]Department of Radiation Oncology (Free Radical and Radiation Biology Program), Carver College of Medicine, The University of Iowa, Iowa City, Iowa;

[f]Department of Chemistry, The University of Iowa, Iowa City, Iowa;

[g]Viewpoint Molecular Targeting, LLC, Coralville, Iowa

Abstract

The use of targeted radionuclide therapy for cancer is on the rise. While beta-particle-emitting radionuclides have been extensively explored for targeted radionuclide therapy, alpha-particle-emitting radionuclides are emerging as effective alternatives. In this context, fundamental understanding of the interactions and dosimetry of these emitted particles with cells in the tumor microenvironment is critical to ascertaining the potential of alpha-particle-emitting radionuclides. One important parameter that can be used to assess these metrics is the S-value. In this study, we characterized several alpha-particle-emitting radionuclides (and their associated radionuclide progeny) regarding S-values in the cellular and tumor-metastasis environments. The Particle and Heavy Ion Transport code System (PHITS) was used to obtain S-values via Monte Carlo simulation for cell and tumor metastasis resulting from interactions with the alpha-particle-emitting radionuclides, lead-212 (^{212}Pb), actinium-225 (^{225}Ac) and bismuth-213 (^{213}Bi); these values were compared to the beta-particle-emitting radionuclides yttrium-90 (^{90}Y) and lutetium-177 (^{177}Lu) and an Auger-electron-emitting radionuclide indium-111 (^{111}In). The effect of cellular internalization on S-value was explored at increasing degree of internalization for each radionuclide. This aspect of S-value determination was further explored in a cell line-specific fashion for six different cancer cell lines based on the cell dimensions obtained by confocal microscopy. S-values from PHITS were in good agreement with MIRDcell S-values (cellular S-

Address for correspondence: University of Iowa, Radiology/Radiation Oncology, ML B180 FRRBP, 500 Newton Road, Iowa City, Iowa 52242; michael-schultz@uiowa.edu.

Editor's note. The online version of this article (DOI: 10.1667/RR15081.1) contains supplementary information that is available to all authorized users.

values) and the values found by Hindié *et al.* (tumor S-values). In the cellular model, ^{212}Pb and ^{213}Bi decay series produced S-values that were 50- to 120-fold higher than ^{177}Lu, while ^{225}Ac decay series analysis suggested S-values that were 240- to 520-fold higher than ^{177}Lu. S-values arising with 100% cellular internalization were two- to sixfold higher for the nucleus when compared to 0% internalization. The tumor dosimetry model defines the relative merit of radionuclides and suggests alpha particles may be effective for large tumors as well as small tumor metastases. These results from PHITS modeling substantiate emerging evidence that alpha-particle-emitting radionuclides may be an effective alternative to beta-particle-emitting radionuclides for targeted radionuclide therapy due to preferred dose-deposition profiles in the cellular and tumor metastasis context. These results further suggest that internalization of alpha-particle-emitting radio-nuclides via radiolabeled ligands may increase the relative biological effectiveness of radiotherapeutics.

INTRODUCTION

Targeted radionuclide therapy (TRT) is recognized as a promising therapeutic modality for several types of inoperable or metastatic cancers (1). One therapeutic strategy for the use of targeted radionuclide therapy takes advantage of known biochemical behavior of elements that results in preferential accumulation of radionuclides in specific malignant lesions. For example, iodine-131 (^{131}I) naturally accumulates in thyroid tissue for thyroid cancer therapy (2); and radium-223 (^{223}Ra), as a calcium analog, accumulates naturally in highly-proliferative prostate-cancer bone metastases (3). A second strategy is to direct radiation to cancer cells using radiolabeled ligands that bind with high affinity to cancer-specific receptors or antigens that are highly expressed on malignant cells in the tumor microenvironment relative to normal cells. In this strategy, tumor targeting is afforded via small molecules (ligand-directed radionuclide therapy), peptides (peptide receptor radionuclide therapy) and radiolabeled antibodies (radio-immuno-therapy) (4–8). One prominent example is somatostatin analog-based peptide receptor radionuclide therapy, which targets highly-expressed somatostatin receptor subtype 2 (SSTR2) for therapy of neuroendocrine tumors. Favorable outcomes relative to current standard-of-care therapy in recent clinical trials suggest a promising future for these agents for the treatment of neuroendocrine tumor patients (9, 10). In this context, among the various considerations required for the development of successful therapeutic strategies, choice of radionuclide is essential (1). For neuroendocrine tumor patient care, indium-111 (^{111}In) was the first radionuclide introduced commercially. 111In was introduced initially as a SSTR2-targeted peptide-based diagnostic [^{111}In-DTPA^{0}-octreotide (also known as Octreo-Scan)], taking advantage of a favorable half-life ($t_{1/2}$ = 2.8 days) and photon emissions that are amenable to imaging via single photon emission computed tomography (SPECT) (11). ^{111}In was later considered as a therapeutic option (at high doses), employing the concomitant low-energy Auger electrons that accompany photon emissions (12–15). More recently, clinical trials of peptide receptor radionuclide therapy for neuroendocrine tumor patients have been conducted using beta-particle-emitting radionuclides yttrium-90 (^{90}Y) and lutetium-177 (^{177}Lu) in the forms of ^{90}Y-DOTA^{0}-Tyr^{3}-octreotide (^{90}Y-DOTATOC) or ^{177}Lu-DOTA^{0}-Tyr^{3}-octreotate (^{177}Lu-DOTATATE) (16–20). While these beta-particle-emitting radionuclides have been extensively investigated and used for clinical trials, the high-linear

energy transfer (LET) of alpha particles is emerging as a less-explored paradigm that represents a promising alternative. Radium-223, the first alpha-particle-emitting radionuclide approved for cancer therapy by the U.S. Food and Drug Administration (FDA) [^{223}Ra dichloride (Xofigo®); Bayer HealthCare Pharmaceuticals Inc., Whippany, NJ], has provided evidence of the promise of alpha-particle therapy for cancer by significantly improving the median overall survival of metastatic castration-resistant prostate-cancer patients (mCRPC), with minimal reported toxicity (3, 21). In contrast, the effectiveness of beta-particle-emitting radionuclides strontium-89 and samarium-153 for this purpose is generally considered to be palliative, with no survival benefit and an accompanying risk of myelosuppression (22). Thus, alpha-particle therapy for cancer is emerging as a promising approach to treatment.

Internal radiation dosimetry to tumors and critical organs (e.g., kidneys) is critical for precise treatment planning and the prediction of therapeutic outcomes for patients undergoing targeted radionuclide therapy. The Medical Internal Radiation Dose (MIRD) schema (23) has been considered a standard dosimetry approach for targeted radionuclide therapy, where the intravenous infusion of radiopharmaceutical is required. The dose can be obtained as the product of cumulative radioactivity within the time of interest and S-value, which is a figure of merit that describes the mean absorbed dose within the organ/tumor per decay of radionuclide from the source region (23). However, in some instances, the absorbed dose to individual cells is more meaningful, particularly when the targeting moiety concentrates in the cells and emits radiation with a path length comparable to dimensions of cells and small tumor metastases. There have been extensive efforts to evaluate the relative merits of various radionuclides available for therapy at the cellular scale using analytic methods or Monte Carlo radiation transport codes (24–34). However, these studies have focused primarily on beta- or Auger-electron emitters, while dosimetry studies of alpha particles in this area are limited.

In this study, we explored the effect of high-LET alpha particles using the S-value determination for direct comparison to beta-particle-emitting radionuclides for cancer therapy. The radionuclides actinium-225 (^{225}Ac), bismuth-213 (^{213}Bi), lead-212 (^{212}Pb) and astatine-211 (^{211}At) are under investigation for ligand-targeting radionuclide based therapies for cancer (35–37). Among these candidates, we selected three alpha-particle emitters (^{225}Ac, ^{213}Bi and ^{212}Pb) and characterized them according to cellular and tumor S-values. We further compared these results to S-values for the widely used beta-particle emitters ^{90}Y and ^{177}Lu, and to the Auger-electron emitter ^{111}In. The dependency of S-values on the degree of internalization was also characterized. Furthermore, we calculated cell line-specific S-values using appropriate cellular and nuclear radii of six human cancer cell lines derived from confocal microscopy images of live cells. The data presented here will assist in dosimetry calculations of novel alpha-particle-emitting radiopharmaceuticals that are being evaluated in the preclinical and clinical settings.

MATERIALS AND METHODS

Particle and Heavy Ion Transport code System (PHITS) software version 2.76 (38) (Japan Atomic Energy Agency, Tokai, Japan) was used to characterize alpha-particle interactions

and to estimate dose deposition for cells and tumor metastases in model systems. These analyses were initiated with validation of PHITS (Supplementary Fig. S3; http://dx.doi.org/10.1667/RR15081.1.S1). The energy depositions per unit path length resulting from the PHITS simulation were compared with the values obtained from available stopping-power acquisition software (39, 40). Figure 1 represents the decay schemes of the radionuclides investigated (^{212}Pb, ^{225}Ac, ^{213}Bi, ^{90}Y, ^{177}Lu and ^{111}In), and Supplementary Table S1 (http://dx.doi.org/10.1667/RR15081.1.S1) summarizes the details of decay characteristics and radiation emissions that were included in our analyses. Decay data employed were obtained from the Radiological Toolbox software version 3.0 (41) (Oak Ridge National Laboratory, Oak Ridge, TN), which incorporates the nuclear decay data of the International Commission on Radiological Protection (ICRP) Publication 107 (42). The radiation-emission data of electrons, including beta particles, internal conversion electrons (CEs) and Auger electrons (Supplementary Fig. S1; http://dx.doi.org/10.1667/RR15081.1.S1), as well as alpha particles (Supplementary Fig. S2; http://dx.doi.org/10.1667/RR15081.1.S1) and photons from each radionuclide, were specified in source definitions. Liquid water was substituted in the geometries of either single sphere or concentric spheres of various sizes for cells and tumor metastases as described elsewhere (26, 33). The cutoff energy of electrons for the simulation was set to 1 keV and a total of 1,000,000 particles were transported for each simulation.

Depth-Dose Distribution of Alpha Particles

The alpha particles of mean energies, as specified in Supplementary Table S1, emitted from the radionuclides investigated were irradiated into a thin water slab (10 cm × 10 cm × 2 cm) and depth-dose distributions were obtained. The branching ratios were taken into account using the global normalization factor, totfact, in the source definition. The LETs (initial and maximum) and ranges were obtained based on the distributions.

Cellular Dosimetry

Two concentric water spheres were constructed representing cellular and nuclear membranes, respectively. Four different cellular sizes, ranging from 3–10-μm radii for the cell membrane and 2–7-μm radii for the nucleus, were selected. The source was assumed to be isotropic and uniformly distributed within the cell compartments [either whole cell (C), nucleus (N) or cytoplasm (Cy)] or on the cell surface (CS). Five different source-to-target combinations, cell to cell (C ← C), cell surface to cell (C ← CS), nucleus to nucleus (N ← N), cytoplasm to nucleus (N ← Cy) and cell surface to nucleus (N ← CS), were considered. Cellular S-values were then obtained for each radionuclide and compared to the values from MIRDcell software version 2.0.16 (43) (Rutgers New Jersey Medical School, Newark, NJ). Because the nuclear transformations of the alpha-particle emitters investigated result in subsequent radionuclide progeny, we had assumed that all daughters of the decay series are retained within the cellular compartment or on the cell surface during the decay processes. Because the MIRDcell S-values are only available for single radionuclides, not for the whole decay series, we added up the respective MIRDcell S-values from each decay daughter within the decay series with appropriate consideration of branching ratios, and compared with the PHITS S-values.

Dose Deposition as a Function of Cellular Internalization

Two concentric spheres of 5-μm and 4-μm radii for cell membrane and nucleus, respectively, were constructed for the dosimetry determinations. In the source definition, two source sections were specified: one for the internalized source and the other for the membrane-bound source. The internalized portion was then increased from 0% (all membrane-bound) to 100% (fully internalized) by 20% increments while the membrane-bound portions were decreased accordingly. S-values were then obtained for cell and nucleus, respectively, as a function of cellular internalization for the radionuclides under investigation.

Cell Line-Specific Dosimetry

To investigate the potential differences in S-values and susceptibility to alpha-particle versus beta-particle dose deposition, the following six human cancer cell lines were investigated: neuroendocrine tumor cells BON-1 and NCI-H727; prostate cancer cells DU-145 and PC-3; and melanoma cells A375 and A2058. A cell imaging study was first performed to establish dimensions of the human cancer cell lines. Cells were cultured in the recommended media supplemented with 10% fetal bovine serum (Gibco®; Life Technologies, Grand Island, NY). Cells ($1.5 – 3.0 \times 10^5$) were seeded in six-well plates with coverslips on the bottom of the plates and cultured for two days. The cells were then stained with CellMas™ Deep Red Plasma Membrane Stain (Molecular Probes®, Eugene, OR) for membrane staining for 10 min at 37°C and fixed with 4% paraformaldehyde. The coverslips were then mounted onto SlowFade™ Gold Antifade reagent with DAPI (Molecular Probes) and allowed to stand overnight at 4°C. The samples were imaged on a Leica SP8 laser scanning confocal microscope (Mannheim, Germany) at The University of Iowa Central Microscopy Research Facility (Iowa City, IA). DAPI and Deep Red membrane stains were excited with 405-nm and 649-nm laser lines, respectively. Due to the irregular morphology of the cancer cells, the volumes of the cells and the nuclear compartments were estimated from confocal z-stacks, using Imaris software V9.0 (Bitplane AG, Zurich, Switzerland), and the radii of spheres from the volume information were derived based on these estimates. The average values were obtained from at least 30 cell images. These realistic cellular dimensions were then used for PHITS calculation for the cell line-specific S-values. The cell and nucleus S-values were calculated from two different source locations: cell (C; 100% internalization) and cell surface (CS; 0% internalization).

Dosimetry for Tumor Metastases of Various Sizes

Water spheres with various diameters ranging from 10 μm to 1 cm, representing tumor metastases of various sizes, were constructed and simulated to obtain S-values for tumor metastases. The source definition was modified to specify either all types of radiations, or a single radiative emission (alpha particles, beta particles, conversion electrons, Auger electrons or photons) at a time, to investigate the relative contribution of each type of radiation to final dose. We compared the PHITS S-values from ^{177}Lu, ^{90}Y and ^{111}In transport determined in this way with the values from Hindié *et al.* (33) and newly reported the PHITS S-values for the alpha-decay series ^{225}Ac, ^{213}Bi and ^{212}Pb.

RESULTS

Depth-Dose Distribution of Alpha Particles

The ranges of all alpha particles emitted from the three alpha-decay series investigated were between 45 μm and 88 μm, which corresponds to multiple cell diameters (Fig. 2). The ^{225}Ac decay series produced four pronounced Bragg peaks with an initial LET of 62 keV μm^{-1} to 83 keV μm^{-1} and a maximum LET of 232 keV μm^{-1} to 238 keV μm^{-1} (Fig. 2A). The alpha particle arising from ^{213}Bi decay was negligible due to the low branching ratio of ^{213}Bi to alpha decay (to ^{209}Tl), which accounts for only 2.1%. The difference in the branching ratios of ^{212}Bi and ^{213}Bi resulted in the different patterns of depth-dose distributions, where the ^{213}Bi decay series produced a single pronounced peak with a maximum LET of 232 keV μm^{-1}, while the ^{212}Pb decay series resulted in two pronounced peaks, with lower maximum LETs of 86 keV μm^{-1} and 153 keV μm^{-1}, respectively (Fig. 2B and C).

Cellular Dosimetry

The observed cellular S-values obtained using PHITS were in good agreement with MIRDcell S-values for the radionuclides under investigation, with percentage differences of less than 6% for all three alpha-decay series evaluated and of less than 13% for ^{177}Lu and ^{90}Y (Fig. 3; Supplementary Tables S2 and S3, http://dx.doi.org/10.1667/RR15081.1.S1). On the other hand, the S-values obtained for ^{111}In were significantly different (up to 36%) from MIRDcell when the source was restricted to the cell surface (Fig. 3; Supplementary Table S2).

In a comparison of alpha-decay series dose deposition, the ^{225}Ac decay series imparted four- to fivefold higher doses to cells than the ^{213}Bi and ^{212}Pb decay series in the cell model (due to an increase in alpha particles emitted in the ^{225}Ac series; Supplementary Table S3). The observed dose depositions of the ^{213}Bi and ^{212}Pb decay series were similar, with the efficiency of the ^{212}Pb decay slightly higher (~10%) than the ^{213}Bi decay series (within the cellular dimensions examined; Supplementary Table S3). Compared to beta-particle emitters, alpha-particle emitters deposited significantly higher doses, imparting 50- to 120-fold higher doses from the ^{212}Pb and ^{213}Bi decay series and 240- to 520-fold higher doses from the ^{225}Ac decay series than the doses deposited by ^{177}Lu (Supplementary Tables S2 and S3). ^{177}Lu $\left(\overline{E}_{\bar{\beta}} = 133 \text{ keV}\right)$ and ^{111}In $\left(\overline{E}_{\text{Auger}} = 0.926 \text{ keV}\right)$ doses were up to 7- and 14-fold higher, respectively, compared to ^{90}Y $\left(\overline{E}_{\bar{\beta}} = 933 \text{ keV}\right)$ (Supplementary Table S2). The ^{111}In dose was highly efficient when the source was localized to the nucleus, while the effect was significantly reduced when the source was positioned on the cell surface (Supplementary Table S2). For example, in a cell comprising a 3-μm radius, when the source was positioned inside the nucleus (N ← N), the ^{111}In dose was 14-fold and 2-fold higher than ^{90}Y and ^{177}Lu, respectively. On the other hand, the effect on dose deposition was reduced significantly (twofold and one-half-fold, respectively) when the ^{111}In source was positioned on the cell surface (N ← CS).

Dose Deposition as a Function of Cellular Internalization

Cellular internalization changed the energy deposition pattern significantly at the cellular level, and the doses to the cell and the nucleus were increased as the internalization of radiopharmaceuticals was increased (Fig. 4A; represented with ^{177}Lu). Our results suggest that the nucleus is more susceptible to internalization than the whole cell, and the degree of increase in dose deposition by the internalization, indicated by increase factors (IFs; the relative ratio between the S-values from 100% vs. 0% internalizations), was radionuclide-dependent (Fig. 4B and C). The doses from alpha-particle emitters were increased by a factor of up to 2.3 to nuclei as internalization was increased from 0% to 100% (Fig. 4B). The effect of percentage internalization of the beta-particle and the Auger-electron emitters on S-values tended to depend on electron energy (Figs. 1 and 4). For example, the IF of ^{111}In for the nucleus was 6.0, while the increase factors of ^{90}Y was 2.1 (Fig. 4B), reflecting the relatively short range of the Auger electrons versus the long range of high-energy beta particles emitted by ^{90}Y.

Cell Line-Specific Dosimetry

The precise dimensions of six different human cancer cell lines (human neuroendocrine tumor cells BON-1 and NCI-H727; prostate cancer cells DU-145 and PC-3; and melanoma cells A375 and A2058) were obtained by confocal microscopy (Fig. 5). The prostate cancer cell lines had the largest cell radii (DU-145: 9.75 ± 0.64 μm; PC-3: 9.14 ± 0.91 μm), followed by the melanoma cell lines (A375: 8.81 ± 0.99 μm; A2058: 8.69 ± 0.72 μm) and the neuroendocrine tumor cell lines (BON-1: 7.76 ± 0.55 μm; NCI-H727: 7.51 ± 0.60 μm). The melanoma cell lines had relatively larger nuclei relative to cell size compared to the other cell lines examined (e.g., R_N/R_C; 0.74 for A375 vs.0.63 for PC-3; Fig. 5). In general, cells were round in shape, except for melanoma cell lines, which were characterized by more variation in shape than the other human cancer cell lines examined. When these cells were well separated (less than 50% confluent), the melanoma cells tended to be flat and elongated, but resolved into a more rounded shape as confluent colonies formed. The cell line-specific S-values obtained from PHITS simulation for each radionuclide are reported in Supplementary Table S4 (http://dx.doi.org/10.1667/RR15081.1.S1). The effective dose deposition of all radionuclide decays was found to be dependent on cell size, i.e., the most effective dose deposition was observed for the NCI-H727 cells (smallest radius), while DU-145 (largest radius) resulted in the lowest dose deposition ($S_{C\leftarrow C}$ with ^{177}Lu; Gy Bq^{-1}s^{-1}; 4.25E–04 for NCI-H727 vs. 2.39E–04 for DU-145; Supplementary Table S4). The melanoma cell lines were less susceptible to internalization as shown by a lower $S_{N\leftarrow C}/S_{N\leftarrow CS}$ ratio (except for the cases from ^{111}In; Supplementary Table S4), which corresponds to the higher R_N/R_C (Fig. 5).

Dosimetry for Tumor Metastases of Various Sizes

The tumor S-values obtained from PHITS were within 6% for ^{177}Lu and ^{90}Y and variable for ^{111}In compared to those of Hindié *et al.* (33) (Fig. 6; Supplementary Table S5, http://dx.doi.org/10.1667/RR15081.1.S1). The difference for ^{111}In in tumor S-value was 3% for the 10-μm-diameter cell, while a 24% difference was observed for the 1-cm-diameter tumor compared to Hindié *et al.*, ostensibly due to an increased contribution from photons (0.3% in

the 10-μm cell vs. 17% in the 1-cm tumor; Supplementary Table S5). When the photon emissions were ignored, as in Hindié *et al.*, the S-values for ^{111}In agreed to within 4% of values obtained by Hindié *et al.*

The observed tumor dose was up to fourfold higher for the ^{225}Ac decay series compared to the ^{212}Pb and ^{213}Bi decay series for all sizes of tumors (Supplementary Table S6, http://dx.doi.org/10.1667/RR15081.1.S1). The ^{212}Pb and ^{213}Bi decay series produced similar dose deposition (less than 10% difference), while the ^{212}Pb decay series produced a slightly higher energy-deposition efficiency than the ^{213}Bi decay series for 100-μm diameter or smaller tumors (Supplementary Table S6). Compared to the beta-particle-emitters ^{177}Lu and ^{90}Y, the alpha-decay series imparted significantly higher doses to all tumors within the size range investigated (Fig. 7; Supplementary Tables S5 and S6). However, as tumor size increased (i.e., ≥1-cm diameter), a highly-localized inhomogeneous dose deposition pattern was observed for the alpha-decay series (Fig. 7A). ^{177}Lu imparted an approximately fivefold higher dose than ^{90}Y for the 10-μm cell, while the higher energy beta-emitter ^{90}Y delivered an approximately fourfold higher dose than ^{177}Lu for larger (1 cm diameter) tumors (Fig. 7; Supplementary Table S5). These results suggest that alpha particles account for most of the dose (≥ 90%) deposited from all alpha-decay series investigated (Fig. 7B; Supplementary Table S6). However, the beta-particle emissions became significant as tumor size increased. Notably, these data indicate that the beta emissions within the alpha-decay series result in similar or higher dose than the pure beta emitters (Fig. 7B).

DISCUSSION

Receptor-targeted radionuclide therapy for cancer is increasingly recognized as a promising approach to cancer treatment. While beta-particle-emitting radionuclides have been explored extensively, alpha-particle-emitting radionuclides are emerging as potentially more effective components of targeted radionuclide therapy radiopharmaceuticals. In this context, characterizing the absorbed dose delivered by these emitted particles within cells in the tumor microenvironment is critical to ascertaining the potential of alpha-particle-emitting radionuclides. One important parameter that can be used to assess these metrics is the S-value. In this study, we examined and characterized several alpha-particle-emitting radionuclides (and their associated radionuclide-progeny) regarding S-values in cellular and tumor-metastasis environments to elucidate their relative merits. The degree of internalization was also assessed for alpha-decay series and compared with beta-particle-emitter interactions.

Monte Carlo simulation codes, including MCNP, PE-NELOPE, GEANT 4 and CELLDOSE, have been used both in cellular and tumor-metastasis dosimetric paradigms for beta-particle- and Auger-electron-emitting radionuclides (29–34), while the alpha-decay series have been largely unexplored within the context of targeted radionuclide therapy. To our knowledge, this is the first reported application of PHITS for cellular and tumor-metastasis dosimetry for alpha particles in the MIRD schema. Thus, this study contributes to a more detailed understanding of dosimetry for emerging applications in targeted alpha-particle therapy for cancer. The results substantiate the benefit of alpha particles versus beta particles for the treatment of cancer. Alpha particles promise a significantly higher dose than beta particles,

particularly at the cellular and tumor-micrometastasis scales. The ranges of alpha particles in the decay series studied were within 45–88 μm (Fig. 2). The physical particle-energy character of alpha particles produces highly localized dose to tumor cells and potentially may result in better tumor control than high-energy beta particles, as indicated in previously published *in vitro* and *in vivo* preclinical studies (44–46). Interestingly, Chan *et al.* (47) reported, based on a study of ^{213}Bi-[DOTA^{0},Tyr^{3}]-octreotate alpha-particle therapy for neuroendocrine tumors in an animal model, that alpha particles were effective in both small (<6 mm diameter) and large (up to 1 cm diameter) tumor sizes. This finding might be explained by high vascularization of the larger tumors, which may provide a more homogeneous distribution of the radiopharmaceutical within the tumor microenvironment, thereby promoting a homogenous cell-killing effect of high-LET alpha particles (along with a potentially high bystander effect). Although these authors considered the contribution from beta-particle dose deposition to be relatively insignificant (less than 5% of total dose), our results suggest that long-ranged energetic electrons within the alpha-decay series are an important contribution for large well-vascularized tumors (Fig. 7B).

Our results show that the highest total absorbed dose deposition to the tumor microenvironment arises from localization of the ^{225}Ac decay series due to four pronounced alpha-particle emissions within the series. These data are aligned with the notion that ^{225}Ac acts as an "*in vivo* generator" due to a relatively long half-life (10 days) with a dose that is highly influenced by the decay of radionuclide progeny in the series. Importantly, these results assume that migration of ^{225}Ac radioactive progeny is negligible. The ^{212}Pb and ^{213}Bi decay series produced a similar pattern of dose deposition in this study, stemming from similar decay schemes, which include two alpha-particle and three beta-particle emissions. However, the difference in half-lives(10.6 h vs. 45.6 min; Fig. 1) of parent nuclei, ^{212}Pb and ^{213}Bi, might lead to a difference in relative biological effectiveness due to the difference in dose rates. In accordance with previously reported observations (33, 48), the relative dose depositions of ^{177}Lu and ^{90}Y as tumor size increases were a function of beta-particle emission energy (Figs. 1 and 7). Thus, the energy of emission is an important criterion for selection of beta emitters for patient therapy (depending on the tumor size) and substantiates that the use of a combination of ^{177}Lu and ^{90}Y might lead to better tumor control, as reported elsewhere (49, 50). In the same way, as a low-energy Auger-electron emitter, the effectiveness of ^{111}In in delivering cytotoxic dose depends greatly on the degree of internalization of ligand (Fig. 4B). The dose contribution of photons has been ignored because of the small contribution to the total dose, typically accounting for <5% (30, 33). However, this study suggests that accurate dosimetry may need to include the contributions of photons when low-energy Auger-electron emitters, such as ^{111}In, are used in relatively large volume tumors (Supplementary Table S5).

The degree of cellular internalization of radioligand in the tumor microenvironment is recognized as an important parameter in predicting the effectiveness of a given receptor-targeted radionuclide therapy (5, 51, 52). This is particularly true for alpha-particle emitters, for which proximity to the nucleus increases the likelihood of alpha-particle interactions with DNA, and catastrophic-unrepairable double-strand breaks that lead to apoptosis of cancer cells in the tumor (53, 54). The efficiency of the radiolabeled ligand-mediated internalization is dependent on the structure of ligand and type of biological target (5, 51,

52). While previously published dosimetry studies have restricted models to source-to-target combinations such as cell to nucleus (N ← C; 100% internalization) and cell surface to nucleus (N ← CS; 0% internalization) (26, 30, 32, 34), our study is unique in the description of S-values that are stratified by increasing degree of radioligand cellular internalization (Fig. 4). Because the internalization of radioligands is rarely 100% (55, 56), we expect this study can contribute to more accurate cellular dosimetry since the cells are likely to display differing degrees of internalization in a cell line-specific and ligand-dependent fashion. Based on our study, further research is required to elucidate the impact on this internalization in the context of antagonists used for therapeutic purposes, since a lower biological effect may arise due to lower dose deposition to the nucleus, which may counterbalance the perceived benefits of antagonists with respect to cell binding.

Sizes of the whole-cell and nucleus are critical parameters for an accurate assessment of absorbed dose, where short-ranged radiations emitted from intracellularly-distributed radionuclides can significantly alter the dose, based on these sizes (30, 57). Here we report on cell line-specific S-values for six different cancer cell lines relevant to targeted radionuclide therapy (Supplementary Table S4). These cell imaging data (Fig. 5; coupled with our S-value determinations) suggest that care should be taken when simplified geometries are employed for dosimetry, i.e., concentric spheres may not adequately describe the geometric dimensions of individual cell lines such as was observed for well-separated melanoma. For example, Sefl *et al.* (32) reported that the difference between a sphere and an irregular shape could result in a significant difference in cellular dose (up to 300%).

A common simplifying assumption in dosimetry analysis for decay series (such as described in this work) is that all decay progeny remain within the same target region as the parent radionuclide (i.e., ^{212}Pb; ^{213}Bi; ^{225}Ac). As pointed out by Kratochwil *et al.* (58), this assumption may contribute to a large uncertainty in the estimation of dosimetry for alpha emitters. That is, the assumption might be valid for some short-lived daughters such as ^{221}Fr (4.8-min half-life) and ^{217}At (33-ms half-life), but might not be valid for relatively long-lived daughters such as ^{213}Bi (45.6-min half-life). As an example, Azure *et al.* (59) investigated the subcellular distribution of ^{212}Pb and its decay daughters along with cellular uptake and biological retention by Chinese hamster V79 cells. Carefully designed studies are required to further elucidate the impact of the migration of progeny from the decay location of parent radionuclides in the tumor microenvironment. Here, we report a separate list of S-values from each daughter nucleus within the alpha-decay series so that the sub-cellular distribution and retention data of each decay daughter (if available) can be taken into account for the precise dosimetry (Supplementary Tables S7 and S8; http://dx.doi.org/10.1667/RR15081.1.S1).

Despite the potential of alpha particles shown in our study (Fig. 7), more preclinical studies are necessary to fully understand the highly dose-localizing nature of the alpha particles for clinical applications. At the microscale, alpha-particle emitters might be distributed non-homogenously, resulting in a highly nonuniform dose distribution over the target region, including critical organs (i.e., kidneys) (60). This heterogeneous dose distribution might be observed to a greater extent than that shown in this study (Fig. 7A; ^{212}Pb for 1-cm tumor),

where the distribution was developed from a uniform distribution of radiopharmaceutical, and might become a potential hurdle for alpha-particle dosimetry.

CONCLUSION

PHITS is a reliable tool to estimate absorbed doses at the cellular and tumor-metastasis scale. This work substantiates the emerging merit of alpha particles versus beta particles that results in significantly higher dose to cancer cells, including large tumor metastases. Results further substantiate that internalization of the alpha-particle-emitting radionuclides via radiolabeled ligands will increase the dose to the nucleus and potentially increase the relative biological effectiveness of radiotherapeutics (although dependent on tumor vasculature). We report cell line-specific S-values for six different cancer cell lines relevant to targeted radionuclide therapy and anticipate that these values can be applied for precise dose estimation in experimental settings.

Supplementary Material

Refer to Web version on PubMed Central for supplementary material.

ACKNOWLEDGMENTS

We thank and acknowledge the following University of Iowa organizations: the Free Radical and Radiation Biology Program, the Holden Comprehensive Cancer Center and the Central Microscopy Research Facility. We especially thank Dr. Yusuf Menda and Dr. Mark Madsen for their review and comments on the paper and Dr. Tatsuhiko Ogawa from the PHITS office for his technical assistance about PHITS simulation. This work was supported by the National Institutes of Health/National Cancer Institute (SPORE grant nos. 1P50CA174521-01A1 and 1K25CA172218-01A1. The authors declare no conflicts of interest in this study. MKS is Chief Science Officer of Viewpoint Molecular Targeting, which has no conflict of interest in the research presented. BB is the Chief Science Officer of Voximetry, LLC, which has no conflict of interest in the research presented.

REFERENCES

1. Gudkov SV, Shilyagina NY, Vodeneev VA, Zvyagin AV. Targeted radionuclide therapy of human tumors. Int J Mol Sci 2015; 17:33.
2. Ruel E, Thomas S, Dinan M, Perkins JM, Roman SA, Sosa JA. Adjuvant radioactive iodine therapy is associated with improved survival for patients with intermediate-risk papillary thyroid cancer. J Clin Endocrinol Metab 2015; 100:1529–36. [PubMed: 25642591]
3. Parker C, Nilsson S, Heinrich D, Helle SI, O'Sullivan JM, Fossa SD, et al. Alpha emitter radium-223 and survival in metastatic prostate cancer. N Engl J Med 2013; 369:213–23. [PubMed: 23863050]
4. Kratochwil C, Giesel FL, Stefanova M, Benesova M, Bronzel M, Afshar-Oromieh A, et al. PSMA-targeted radionuclide therapy of metastatic castration-resistant prostate cancer with 177Lu-labeled PSMA-617. J Nucl Med 2016; 57:1170–6. [PubMed: 26985056]
5. Reubi JC. Peptide receptors as molecular targets for cancer diagnosis and therapy. Endocr Rev 2003; 24:389–427. [PubMed: 12920149]
6. Dash A, Chakraborty S, Pillai MR, Knapp FF Jr. Peptide receptor radionuclide therapy: an overview. Cancer Biother Radiopharm 2015; 30:47–71. [PubMed: 25710506]
7. Larson SM, Carrasquillo JA, Cheung NK, Press OW. Radio-immunotherapy of human tumours. Nat Rev Cancer 2015; 15:347–60. [PubMed: 25998714]
8. Milenic DE, Brady ED, Brechbiel MW. Antibody-targeted radiation cancer therapy. Nat Rev Drug Discov 2004; 3:488–99. [PubMed: 15173838]

9. Kwekkeboom DJ, Kam BL, van Essen M, Teunissen JJ, van Eijck CH, Valkema R, et al. Somatostatin-receptor-based imaging and therapy of gastroenteropancreatic neuroendocrine tumors. Endocr Relat Cancer 2010; 17:R53–73. [PubMed: 19995807]
10. Bergsma H, van Vliet EI, Teunissen JJ, Kam BL, de Herder WW, Peeters RP, et al. Peptide receptor radionuclide therapy (PRRT) for GEP-NETs. Best Pract Res Clin Gastroenterol 2012; 26:867–81. [PubMed: 23582925]
11. Balon HR, Goldsmith SJ, Siegel BA, Silberstein EB, Krenning EP, Lang O, et al. Procedure guideline for somatostatin receptor scintigraphy with 111In-pentetreotide. J Nucl Med 2001; 42:1134–8. [PubMed: 11438641]
12. Krenning EP, Kooij PP, Bakker WH, Breeman WA, Postema PT, Kwekkeboom DJ, et al. Radiotherapy with a radiolabeled somatostatin analogue, [111In-DTPA-D-Phe1]-octreotide. A case history. Ann N Y Acad Sci 1994; 733:496–506. [PubMed: 7978900]
13. Meyers MO, Anthony LB, McCarthy KE, Drouant G, Maloney TJ, Espanan GD, et al. High-dose indium 111In pentetreotide radiotherapy for metastatic atypical carcinoid tumor. South Med J 2000; 93:809–11. [PubMed: 10963516]
14. Anthony LB, Woltering EA, Espenan GD, Cronin MD, Maloney TJ, McCarthy KE. Indium-111-pentetreotide prolongs survival in gastroenteropancreatic malignancies. Semin Nucl Med 2002; 32:123–32. [PubMed: 11965607]
15. Delpassand ES, Sims-Mourtada J, Saso H, Azhdarinia A, Ashoori F, Torabi F, et al. Safety and efficacy of radionuclide therapy with high-activity In-111 pentetreotide in patients with progressive neuroendocrine tumors. Cancer Biother Radiopharm 2008; 23:292–300. [PubMed: 18593362]
16. Bushnell DL Jr., O'Dorisio TM, O'Dorisio MS, Menda Y, Hicks RJ, Van Cutsem E, et al. 90Y-edotreotide for metastatic carcinoid refractory to octreotide. J Clin Oncol 2010; 28:1652–9. [PubMed: 20194865]
17. Imhof A, Brunner P, Marincek N, Briel M, Schindler C, Rasch H, et al. Response, survival, and long-term toxicity after therapy with the radiolabeled somatostatin analogue [90Y-DOTA]-TOC in metastasized neuroendocrine cancers. J Clin Oncol 2011; 29:2416–23. [PubMed: 21555692]
18. Marincek N, Jorg AC, Brunner P, Schindler C, Koller MT, Rochlitz C, et al. Somatostatin-based radiotherapy with [90YDOTA]-TOC in neuroendocrine tumors: long-term outcome of a phase I dose escalation study. J Transl Med 2013; 11:17. [PubMed: 23320604]
19. Kwekkeboom DJ, de Herder WW, Kam BL, van Eijck CH, van Essen M, Kooij PP, et al. Treatment with the radiolabeled somatostatin analog [177Lu-DOTA 0,Tyr3]octreotate: toxicity, efficacy, and survival. J Clin Oncol 2008; 26:2124–30. [PubMed: 18445841]
20. Strosberg J, El-Haddad G, Wolin E, Hendifar A, Yao J, Chasen B, et al. Phase 3 trial of 177Lu-dotatate for midgut neuroendocrine tumors. N Engl J Med 2017; 376:125–35. [PubMed: 28076709]
21. Kluetz PG, Pierce W, Maher VE, Zhang H, Tang S, Song P, et al. Radium Ra 223 dichloride injection: U.S. Food and Drug Administration drug approval summary. Clin Cancer Res 2014; 20:9–14. [PubMed: 24190979]
22. Shore ND. Radium-223 dichloride for metastatic castration-resistant prostate cancer: the urologist's perspective. Urology 2015; 85:717–24. [PubMed: 25681834]
23. Bolch WE, Eckerman KF, Sgouros G, Thomas SR. MIRD Pamphlet No. 21: a generalized schema for radiopharmaceutical dosimetry—standardization of nomenclature. J Nucl Med 2009; 50:477–84. [PubMed: 19258258]
24. Bardies M, Chatal JF. Absorbed doses for internal radiotherapy from 22 beta-emitting radionuclides: beta dosimetry of small spheres. Phys Med Biol 1994; 39:961–81. [PubMed: 15551573]
25. Faraggi M, Gardin I, Stievenart JL, Bok BD, Le Guludec D. Comparison of cellular and conventional dosimetry in assessing self-dose and cross-dose delivered to the cell nucleus by electron emissions of 99mTC, 123I, 111In, 67Ga and 201Tl. Eur J Nucl Med 1998; 25:205–14. [PubMed: 9580851]

26. Goddu SM, Howell RW, Rao DV. Cellular dosimetry: absorbed fractions for monoenergetic electron and alpha particle sources and S-values for radionuclides uniformly distributed in different cell compartments. J Nucl Med 1994; 35:303–16. [PubMed: 8295004]
27. Goddu SM, Rao DV, Howell RW. Multicellular dosimetry for micrometastases: dependence of self-dose versus cross-dose to cell nuclei on type and energy of radiation and subcellular distribution of radionuclides. J Nucl Med 1994; 35:521–30. [PubMed: 8113908]
28. Li WB, Friedland W, Pomplun E, Jacob P, Paretzke HG, Lassmann M, et al. Track structures and dose distributions from decays of 131I and 125I in and around water spheres simulating micrometastases of differentiated thyroid cancer. Radiat Res 2001; 156:419–29. [PubMed: 11554854]
29. Champion C, Zanotti-Fregonara P, Hindie E. CELLDOSE: a Monte Carlo code to assess electron dose distribution—S values for 131I in spheres of various sizes. J Nucl Med 2008; 49:151–7. [PubMed: 18077517]
30. Cai Z, Pignol JP, Chan C, Reilly RM. Cellular dosimetry of 111In using Monte Carlo N-particle computer code: comparison with analytic methods and correlation with in vitro cytotoxicity. J Nucl Med 2010; 51:462–70. [PubMed: 20150261]
31. Falzone N, Fernandez-Varea JM, Flux G, Vallis KA. Monte Carlo evaluation of Auger electron-emitting theranostic tadionuclides. J Nucl Med 2015; 56:1441–6. [PubMed: 26205298]
32. Sefl M, Incerti S, Papamichael G, Emfietzoglou D. Calculation of cellular S-values using Geant4-DNA: The effect of cell geometry. Appl Radiat Isot 2015; 104:113–23. [PubMed: 26159660]
33. Hindié E, Zanotti-Fregonara P, Quinto MA, Morgat C, Champion C. Dose deposits from 90Y, 177Lu, 111In, and 161Tb in micrometastases of various sizes: implications for radiopharmaceutical therapy. J Nucl Med 2016; 57:759–64. [PubMed: 26912441]
34. Cai Z, Kwon YL, Reilly RM. Monte Carlo N-Particle (MCNP) modeling of the cellular dosimetry of 64Cu: comparison with MIRDcell S values and implications for studies of its cytotoxic effects. J Nucl Med 2017; 58:339–45. [PubMed: 27660146]
35. Wadas TJ, Pandya DN, Solingapuram Sai KK, Mintz A. Molecular targeted alpha-particle therapy for oncologic applications. AJR Am J Roentgenol 2014; 203:253–60. [PubMed: 25055256]
36. Dekempeneer Y, Keyaerts M, Krasniqi A, Puttemans J, Muyldermans S, Lahoutte T, et al. Targeted alpha therapy using short-lived alpha-particles and the promise of nanobodies as targeting vehicle. Expert Opin Biol Ther 2016; 16:1035–47. [PubMed: 27145158]
37. Sgouros G, Roeske JC, McDevitt MR, Palm S, Allen BJ, Fisher DR, et al. MIRD Pamphlet No. 22 (abridged): radiobiology and dosimetry of alpha-particle emitters for targeted radionuclide therapy. J Nucl Med 2010; 51:311–28. [PubMed: 20080889]
38. Sato T, Niita K, Matsuda N, Hashimoto S, Iwamoto Y, Noda S, et al. Particle and Heavy Ion Transport code System, PHITS, version 2.52. J Nucl Sci Technol 2013; 50:913–23.
39. Berger MJ, Coursey JS, Zucker DS, Chang J. ESTAR, PSTAR, and ASTAR: computer programs for calculating stopping-power and range tables for electrons, protons, and helium ions. Version 1.2.4 [software]. Gaithersburg: National Institute of Standards and Technology; 1998 (http://physics.nist.gov/Star)
40. Ziegler JF, Ziegler MD, Biersack JP. SRIM - the stopping and range of ions in matter (2010). Nucl Instrum Methods Phys Res B 2010; 268:1818–23.
41. Eckerman KF, Sjoreen AL. The Radiological Toolbox software. Version 3.0 [software]. Oak Ridge: Oak Ridge National Laboratory; 2013 (https://www.ornl.gov/crpk/software)
42. Eckerman K, Endo A. ICRP Publication 107. Nuclear decay data for dosimetric calculations. Ann ICRP 2008; 38:7–96. [PubMed: 19285593]
43. Vaziri B, Wu H, Dhawan AP, Du P, Howell RW, SNMMI MIRD Committee. MIRD pamphlet No. 25: MIRDcell V2.0 software tool for dosimetric analysis of biologic response of multicellular populations. J Nucl Med 2014; 55:1557–64. [PubMed: 25012457]
44. Chan HS, de Blois E, Morgenstern A, Bruchertseifer F, de Jong M, Breeman W, et al. In Vitro comparison of 213Bi- and 177Lu-radiation for peptide receptor radionuclide therapy. PLoS One 2017; 12:e0181473. [PubMed: 28732021]

45. Friesen C, Glatting G, Koop B, Schwarz K, Morgenstern A, Apostolidis C, et al. Breaking chemoresistance and radioresistance with [213Bi]anti-CD45 antibodies in leukemia cells. Cancer Res 2007; 67:1950–8. [PubMed: 17332322]
46. Wild D, Frischknecht M, Zhang H, Morgenstern A, Bruchertseifer F, Boisclair J, et al. Alpha- versus beta-particle radiopeptide therapy in a human prostate cancer model (213Bi-DOTA-PESIN and 213Bi-AMBA versus 177Lu-DOTA-PESIN). Cancer Res 2011; 71:1009–18. [PubMed: 21245097]
47. Chan HS, Konijnenberg MW, de Blois E, Koelewijn S, Baum RP, Morgenstern A, et al. Influence of tumour size on the efficacy of targeted alpha therapy with 213Bi-[DOTA0,Tyr3]-octreotate. EJNMMI Res 2016; 6:6. [PubMed: 26791386]
48. O'Donoghue JA, Bardies M, Wheldon TE. Relationships between tumor size and curability for uniformly targeted therapy with beta-emitting radionuclides. J Nucl Med 1995; 36:1902–9. [PubMed: 7562062]
49. de Jong M, Breeman WA, Valkema R, Bernard BF, Krenning EP. Combination radionuclide therapy using 177Lu- and 90Y-labeled somatostatin analogs. J Nucl Med 2005; 46:S13–7.
50. Kunikowska J, Krolicki L, Hubalewska-Dydejczyk A, Mikolajczak R, Sowa-Staszczak A, Pawlak D. Clinical results of radionuclide therapy of neuroendocrine tumours with 90Y-DOTATATE and tandem 90Y/177Lu-DOTATATE: which is a better therapy option? Eur J Nucl Med Mol Imaging 2011; 38:1788–97. [PubMed: 21553086]
51. Cescato R, Schulz S, Waser B, Eltschinger V, Rivier JE, Wester HJ, et al. Internalization of sst2, sst3, and sst5 receptors: effects of somatostatin agonists and antagonists. J Nucl Med 2006; 47:502–11. [PubMed: 16513620]
52. De Jong M, Valkema R, Jamar F, Kvols LK, Kwekkeboom DJ, Breeman WA, et al. Somatostatin receptor-targeted radionuclide therapy of tumors: preclinical and clinical findings. Semin Nucl Med 2002; 32:133–40. [PubMed: 11965608]
53. Kratochwil C, Giesel FL, Bruchertseifer F, Mier W, Apostolidis C, Boll R, et al. 213Bi-DOTATOC receptor-targeted alpha-radionuclide therapy induces remission in neuroendocrine tumours refractory to beta radiation: a first-in-human experience. Eur J Nucl Med Mol Imaging 2014; 41:2106–19. [PubMed: 25070685]
54. Graf F, Fahrer J, Maus S, Morgenstern A, Bruchertseifer F, Venkatachalam S, et al. DNA double strand breaks as predictor of efficacy of the alpha-particle emitter Ac-225 and the electron emitter Lu-177 for somatostatin receptor targeted radiotherapy. PLoS One 2014; 9:e88239. [PubMed: 24516620]
55. De Jong M, Bernard BF, De Bruin E, Van Gameren A, Bakker WH, Visser TJ, et al. Internalization of radiolabelled [DTPA0]octreotide and [DOTA0,Tyr3]octreotide: peptides for somatostatin receptor-targeted scintigraphy and radionuclide therapy. Nucl Med Commun 1998; 19:283–8. [PubMed: 9625504]
56. Storch D, Behe M, Walter MA, Chen J, Powell P, Mikolajczak R, et al. Evaluation of [99mTc/EDDA/HYNIC0]octreotide derivatives compared with [111In-DOTA0,Tyr3, Thr8]octreotide and [111In-DTPA0]octreotide: does tumor or pancreas uptake correlate with the rate of internalization? J Nucl Med 2005; 46:1561–9. [PubMed: 16157541]
57. Howell RW, Rao DV, Hou DY, Narra VR, Sastry KS. The question of relative biological effectiveness and quality factor for auger emitters incorporated into proliferating mammalian cells. Radiat Res 1991; 128:282–92. [PubMed: 1961925]
58. Kratochwil C, Bruchertseifer F, Rathke H, Bronzel M, Apostolidis C, Weichert W, et al. Targeted alpha-therapy of metastatic castration-resistant prostate cancer with 225Ac-PSMA-617: dosimetry estimate and empiric dose finding. J Nucl Med 2017; 58:1624–31. [PubMed: 28408529]
59. Azure MT, Archer RD, Sastry KS, Rao DV, Howell RW. Biological effect of lead-212 localized in the nucleus of mammalian cells: role of recoil energy in the radiotoxicity of internal alpha-particle emitters. Radiat Res 1994; 140:276–83. [PubMed: 7938477]
60. Sgouros G, Hobbs RF, Song H Modelling and dosimetry for alpha-particle therapy. Curr Radiopharm 2011; 4:261–5. [PubMed: 22201712]

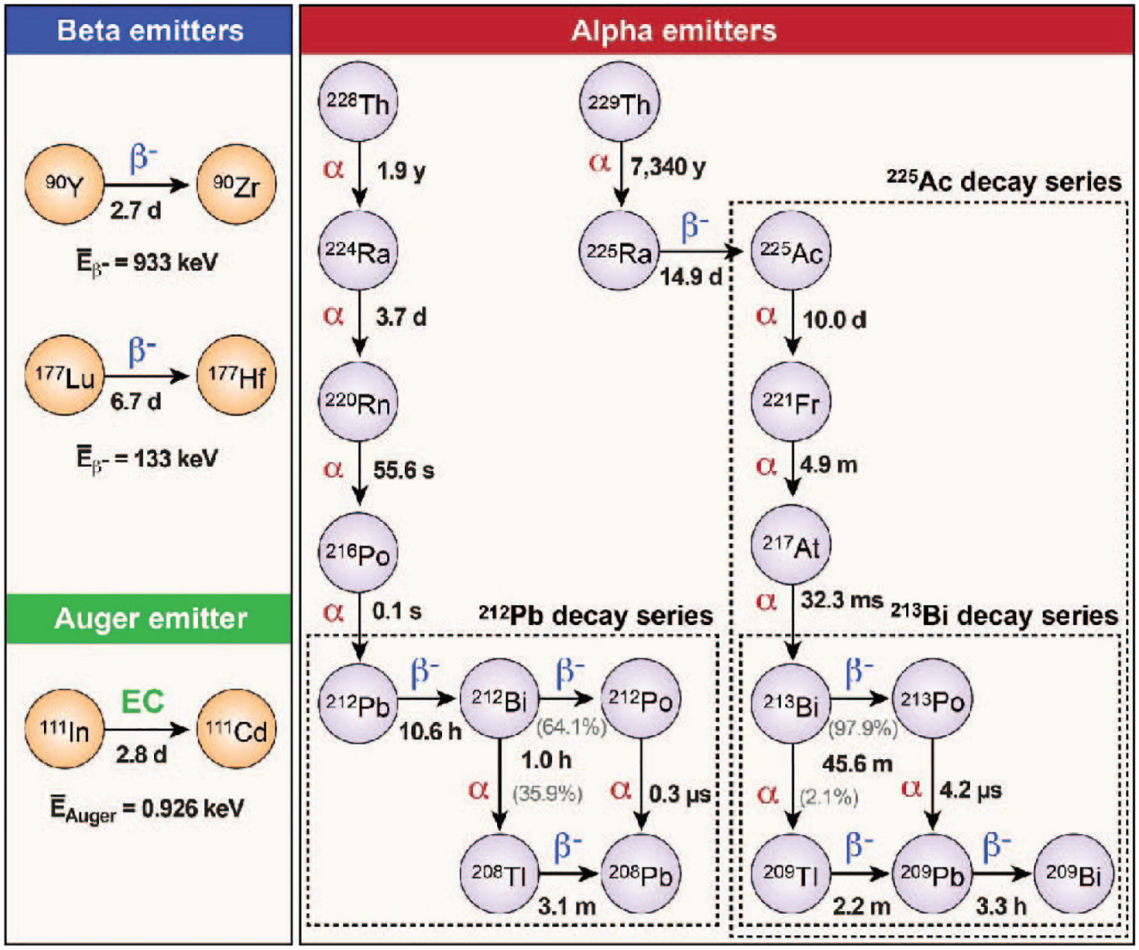

FIG. 1.

Decay schemes of the radionuclides investigated. Two beta-particle-emitting radionuclides ^{90}Y and ^{177}Lu, one Auger-electron-emitting radionuclide ^{111}In and three alpha-particle-emitting radionuclides ^{212}Pb, ^{225}Ac, and ^{213}Bi were included for this study. Note ^{213}Bi is one of the downstream radionuclides of ^{225}Ac decay.

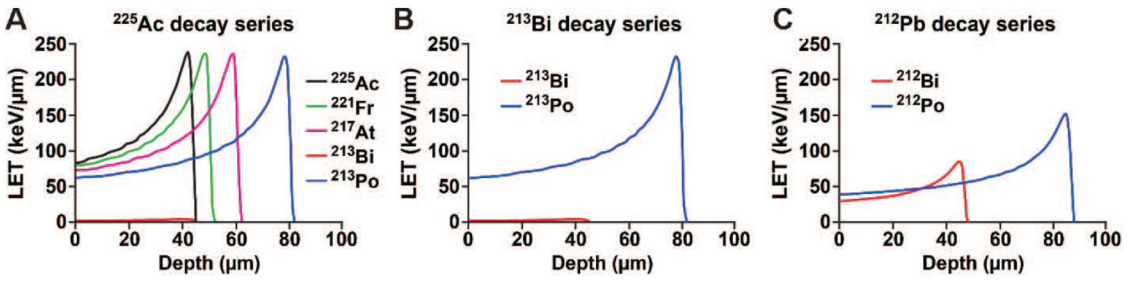

Nuclide	LET (keV/μm)		Range (μm)
	Initial	Max.	
^{225}Ac	82.8	238.3	45
^{221}Fr	78.7	237.2	53
^{217}At	71.8	237.1	63
^{213}Bi	1.7	5.0	47
^{213}Po	61.9	232.4	83

Nuclide	LET (keV/μm)		Range (μm)
	Initial	Max.	
^{213}Bi	1.7	5.0	47
^{213}Po	61.9	232.4	83

Nuclide	LET (keV/μm)		Range (μm)
	Initial	Max.	
^{212}Bi	29.0	85.5	49
^{212}Po	38.5	152.7	88

FIG. 2.

Depth-dose distributions of the alpha particles emitted per decay of (panels A–C, respectively) ^{212}Pb, ^{225}Ac and ^{213}Bi decay series in water slabs. The initial and maximum LETs and corresponding ranges of the alpha particles were determined based on the distributions. The branching ratios were considered.

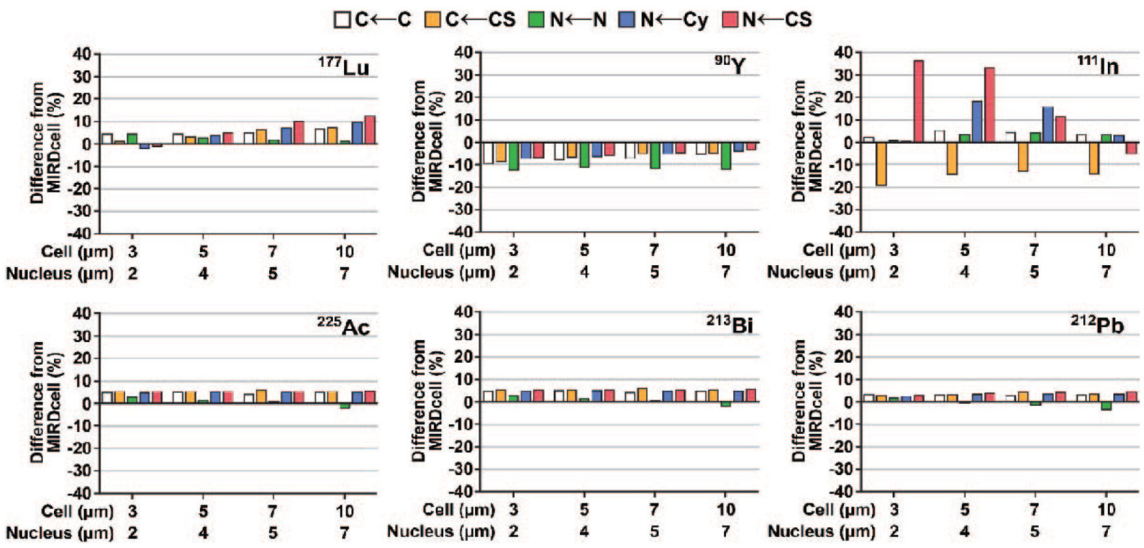

FIG. 3.

Percentage difference between cellular S-values obtained from PHITS simulation and MIRDcell software version 2.0.16 (43) for the radionuclides investigated.

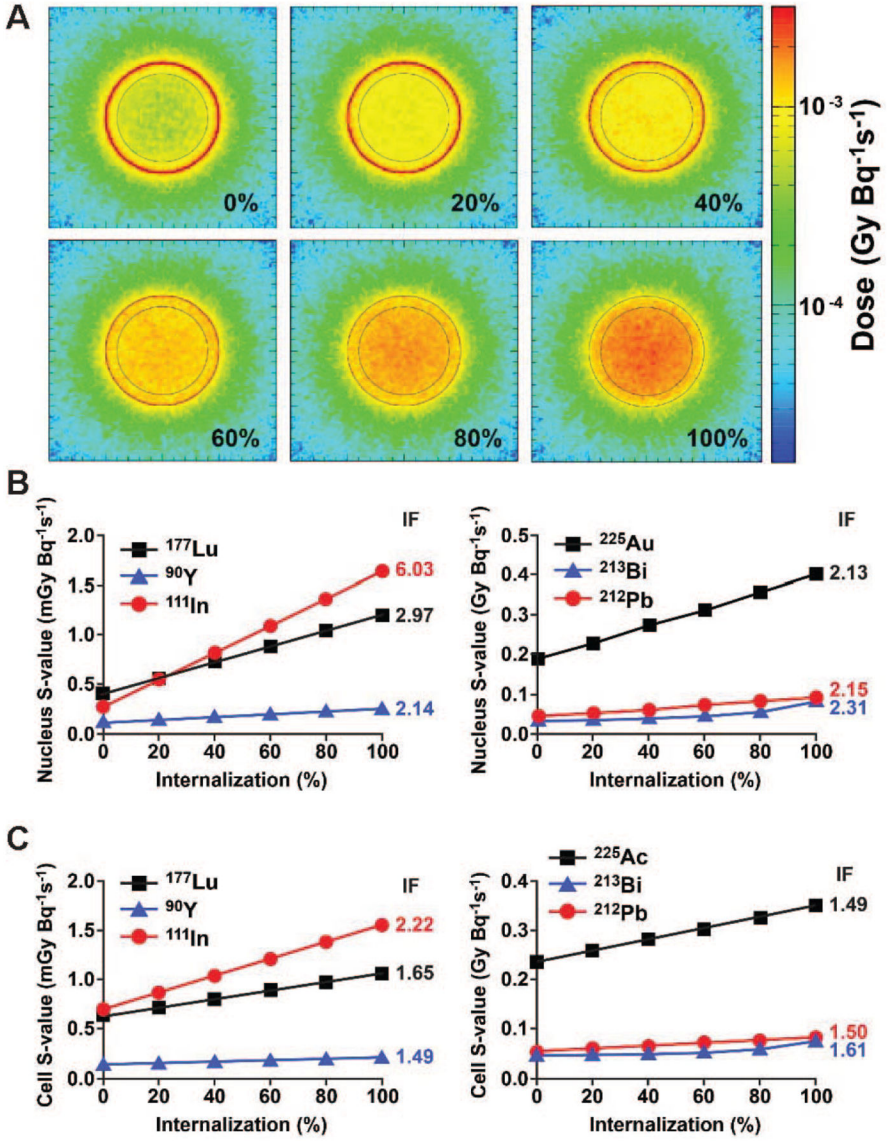

FIG. 4.

Dose deposition as a function of cellular internalization. Panel A: Cross-sectional dose deposition resulted from ^{177}Lu with increasing degree of internalization (by 20% increment). The effect of internalization of the radionuclides investigated on S-values for the nucleus (panel B) and whole cell model (panel C). The ratios between the S-values from 100% vs. 0% internalization are represented as increase factor (IF) on the right sides of the graphs.

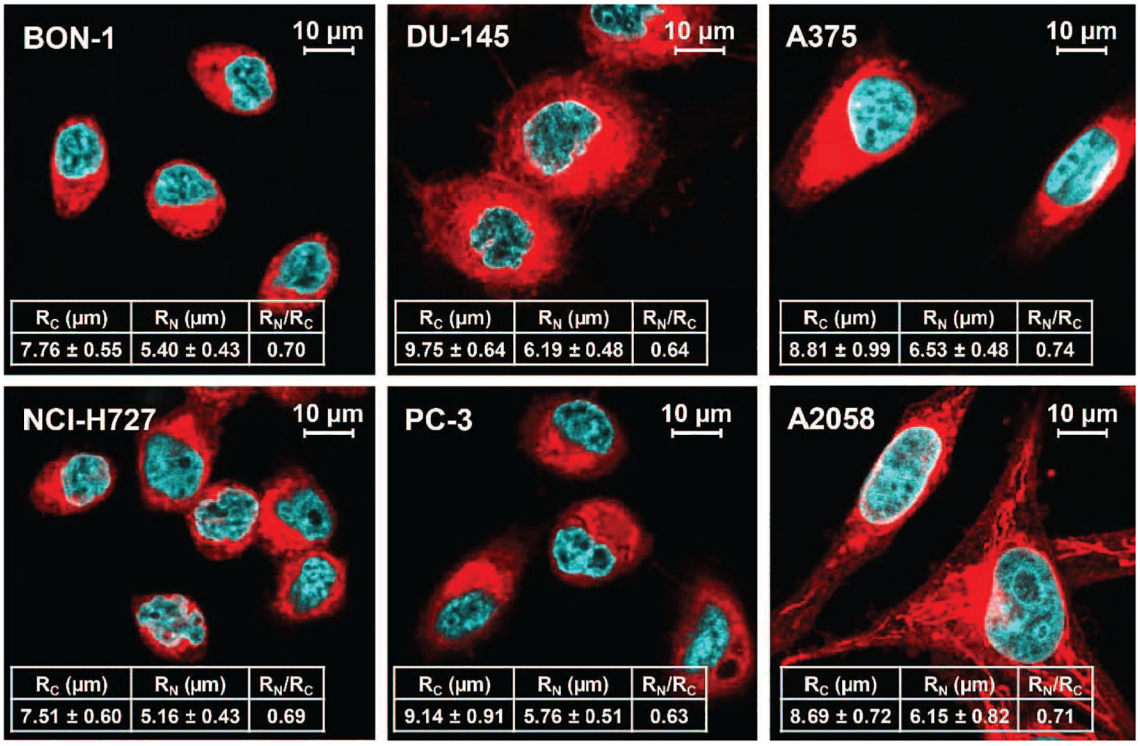

FIG. 5.

Confocal microscopy images of six human cancer cell lines. Averaged volumes of the cells and the nuclei were estimated from confocal z-stacks (at least 30-cell images) and translated to the radii of the cell (R_C) and the nucleus (R_N) assuming the cell and the nucleus were in sphere shapes. R_N/R_C represents the ratio between the cell and the nucleus radii and is regarded as a parameter for susceptibility from internalization.

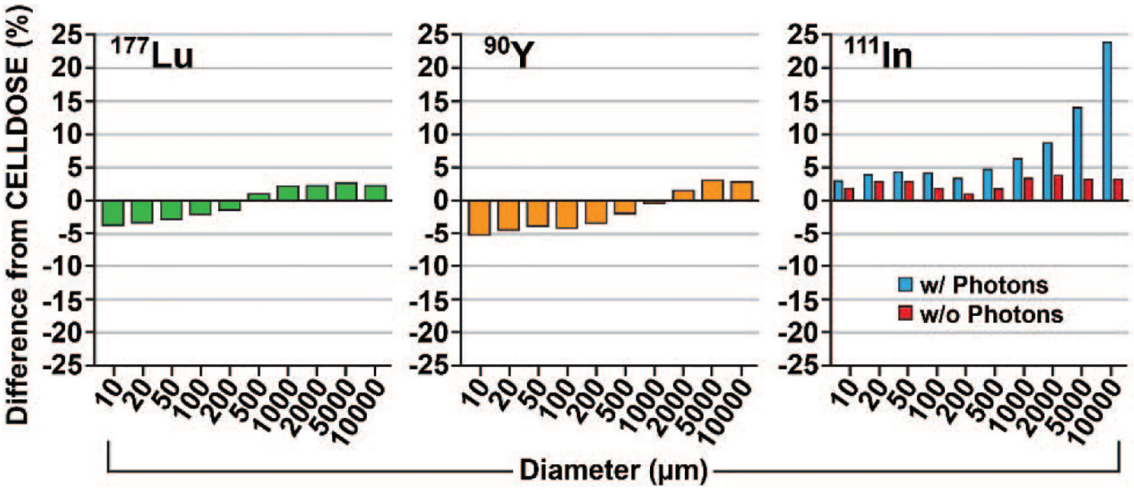

FIG. 6.

Percentage difference between the tumor S-values obtained from PHITS simulation and from Hindié *et al.* (33) for ^{177}Lu, ^{90}Y and ^{111}In. Simulations were repeated for ^{111}In with and without photon specification in the source section.

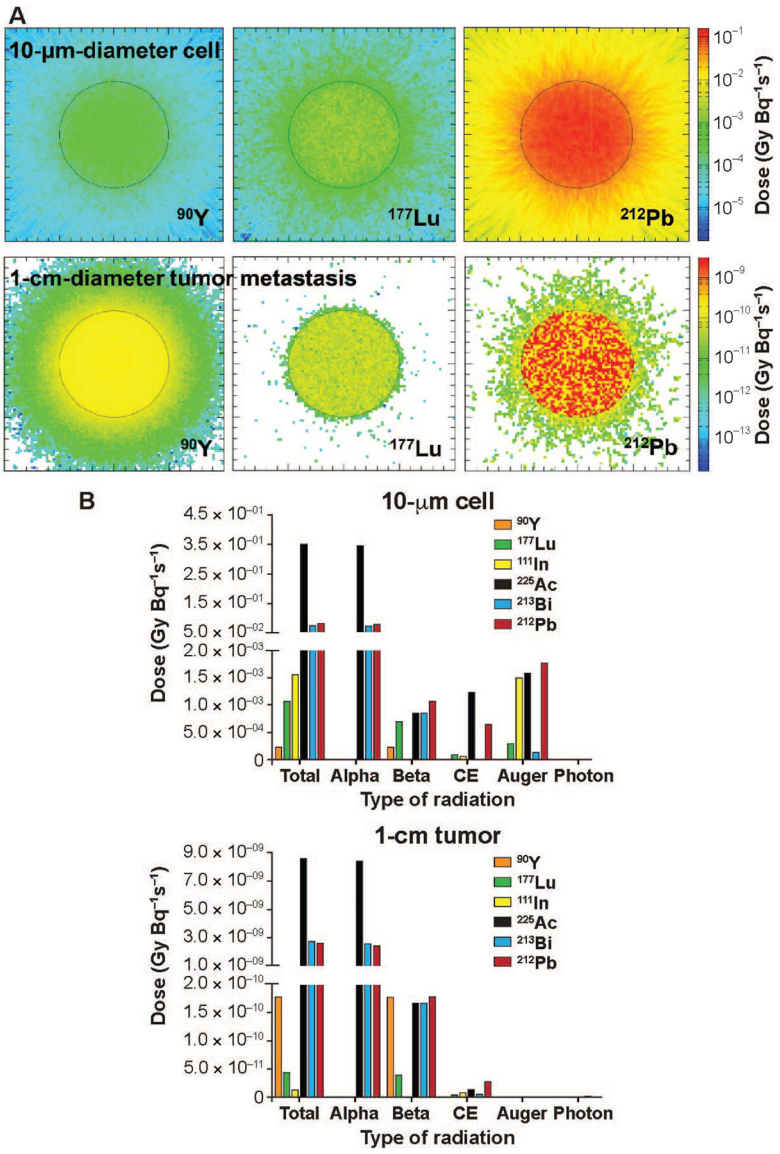

FIG. 7.

Dose deposition to 10-μm-diameter cell vs. 1-cm-diameter tumor metastasis and contribution of each type of radiation to final dose from the decays of radionuclides investigated. Panel A: Cross-sectional dose depositions in 10-μm cells (upper panels) and 1-cm tumor metastases (lower panels) resulted from the decays of beta-particle-emitting radionuclides ^{90}Y and ^{177}Lu, and ^{212}Pb decay series as a representative of the alpha-decay series. Panel B: Radiation dose deposited and each type of radiation emitted from the radionuclides under investigation in 10-μm cells (left panel) and 1-cm tumor metastases (right panel).